Estimation of the error on the calculation of the pressure-strain term: application in the terrestrial magnetosphere

Owen Wyn Roberts[1], Zoltán Voros[1], Klaus Torkar[1], Julia E. Stawarz[2], Riddhi Bandyopadhyay[3], Daniel J Gershman[4], Yasuhito Narita[1], Rungployphan Kieokaew[5], Benoit Lavraud[6], Kristopher Gregory Klein[7], Yan Yang[8], Rumi Nakamura[9], Alexandros Chasapis[10], and William H. Matthaeus[8]

[1]Space Research Institute, Austrian Academy of Sciences
[2]Northumbria University
[3]Princeton University
[4]NASA Goddard Space Flight Center
[5]Institut de Recherche en Astrophysique et Planétologie
[6]Laboratoire d'astrophysique de Bordeaux
[7]University of Arizona
[8]University of Delaware
[9]Space Research Institute
[10]University of Colorado

April 16, 2023

Abstract

Calculating the pressure-strain terms has recently been performed to quantify energy conversion between the bulk flow energy and the internal energy of plasmas. It has been applied to numerical simulations and satellite data from the Magnetospheric MultiScale Mission. The method requires spatial gradients of the velocity and the use of the full pressure tensor. Here we present a derivation of the errors associated with calculating the pressure-strain terms from multi-spacecraft measurements and apply it to previously studied examples of magnetic reconnection at the magnetopause and the magnetotail. The errors are small in a dense magnetosheath event but much larger in the more tenuous magnetotail. This is likely due to larger counting statistics in the dense plasma at the magnetopause than in the magnetotail. The propagated errors analyzed in this work are important to understand uncertainties of energy conversion measurements in space plasmas and have applications to current and future multi-spacecraft missions.

Estimation of the error on the calculation of the pressure-strain term: application in the terrestrial magnetosphere

O.W. Roberts[1], Z. Vörös[1,2], K. Torkar[1], J.Stawarz[3], R. Bandyopadhyay[4], D.J. Gershman[5], Y. Narita[1], R. Kieokaew[6], B. Lavraud[6,7], K. Klein[8], Y. Yang[9], R. Nakamura[1], A. Chasapis[10] and W.H. Matthaeus[9]

[1]Space Research Institute, Austrian Academy of Sciences, Graz, Austria
[2]Institute of Earth's Physics and Space Science, ELRN, Sopron, Hungary
[3]Department of Mathematics, Physics and Electrical Engineering, Northumbria University, Newcastle upon Tyne, NE1 8ST, UK
[4]Department of Astrophysical Sciences, Princeton University, Princeton, NJ 08544, USA
[5]NASA Goddard Space Flight Center, Greenbelt, MD, USA
[6]Institut de Recherche en Astrophysique et Planétologie, CNRS, UPS, CNES, Université de Toulouse, Toulouse, France
[7]Laboratoire d'Astrophysique de Bordeaux, CNRS, University of Bordeaux, Pessac, France
[8]Lunar and Planetary Laboratory, University of Arizona, Tucson, AZ, USA
[9]Department of Physics and Astronomy and Bartol Research Institute, University of Delaware, Newark, Delaware 19716, USA
[10]Laboratory for Atmospheric and Space Physics, University of Colorado Boulder, Boulder, CO, USA

Key Points:

- We estimate the errors on the pressure strain terms calculated from the Magnetospheric MultiScale Mission
- The errors are estimated using two methods, standard error propagation from the velocity and temperature errors and a Monte Carlo method
- Two applications are given using MMS data at the magnetopause and in the magnetotail of Earth

Corresponding author: Owen Wyn Roberts, `owen.roberts@oeaw.ac.at`

Abstract

Calculating the pressure-strain terms has recently been performed to quantify energy conversion between the bulk flow energy and the internal energy of plasmas. It has been applied to numerical simulations and satellite data from the Magnetospheric MultiScale Mission. The method requires spatial gradients of the velocity and the use of the full pressure tensor. Here we present a derivation of the errors associated with calculating the pressure-strain terms from multi-spacecraft measurements and apply it to previously studied examples of magnetic reconnection at the magnetopause and the magnetotail. The errors are small in a dense magnetosheath event but much larger in the more tenuous magnetotail. This is likely due to larger counting statistics in the dense plasma at the magnetopause than in the magnetotail. The propagated errors analyzed in this work are important to understand uncertainties of energy conversion measurements in space plasmas and have applications to current and future multi-spacecraft missions.

1 Introduction

Space plasma processes are often inherently three-dimensional, and single-point measurements cannot distinguish between spatial and temporal changes. Therefore, to better understand space plasma phenomena, multi-point missions such as Cluster (Escoubet et al., 1997, 2001), the Time History of Events and Macroscale Interactions during Substorms (THEMIS) (Angelopoulos, 2008), Swarm (Friis-Christensen et al., 2008), the Magnetospheric MultiScale Mission (MMS) (Burch et al., 2016), and HelioSwarm (Klein et al., 2019) were conceived. Along with the missions, several multi-point methods were developed (M. Dunlop et al., 1988; Paschmann, 1998; Paschmann & Daly, 2008). These include multi spacecraft wave analysis methods (Pincon & Lefeuvre, 1991; Dudok de Wit et al., 1995; Glassmeier et al., 2001; Constantinescu, 2007; Vogt, Narita, & Constantinescu, 2008; Narita et al., 2010; Motschmann et al., 1996; O. Roberts et al., 2014; O. W. Roberts et al., 2017; Narita et al., 2011, 2021), multi-point structure functions (Chen et al., 2010; O. W. Roberts et al., 2022; Pecora et al., 2023), multi-point correlation functions (Horbury, 2000; Matthaeus et al., 2005; K. T. Osman & Horbury, 2007; K. Osman & Horbury, 2009; Bandyopadhyay, Matthaeus, Chasapis, et al., 2020), and magnetic field reconstruction (Denton et al., 2020; Broeren et al., 2021; Denton et al., 2022).

Tetrahedral configurations used on Cluster and MMS allow the calculation of spatial gradients and curls in the plasma. The current density can be estimated by calculating the curl of the magnetic field. This method is termed the curlometer method (M. Dunlop et al., 1988; M. W. Dunlop et al., 2002; Perri et al., 2017; M. W. Dunlop et al., 2021). The curlometer method has often been applied to Cluster magnetic field (M. W. Dunlop et al., 2002; Perrone et al., 2016, 2017; M. W. Dunlop et al., 2021), and velocity data (Kieokaew & Foullon, 2019) where some assumptions are required as ion data is not available on all spacecraft. The curlometer method has also been applied to MMS magnetic field data (Lavraud et al., 2016; Phan et al., 2016; Gershman et al., 2018; Wang et al., 2019). The MMS spacecraft provides multi-point magnetic field data and high-time resolution plasma data, which allows comparison of the curlometer current to the current measured from the plasma data (Lavraud et al., 2016; Phan et al., 2016; Gershman et al., 2018). The multi-point high-time resolution of plasma data has also allowed calculations of the vorticity using the full four spacecraft plasma data (Wang et al., 2019; Zhang et al., 2020).

The plasma heating and energization mechanisms are crucial to understanding several processes, such as plasma turbulence and reconnection. Because of the spatiotemporal ambiguity, it is not always apparent whether temperature increases are due to changing environments, e.g., crossing into a hotter region rather than local heating. The pressure-strain methodology (Del Sarto et al., 2016; Yang, Matthaeus, Parashar, Haggerty, et al., 2017; Yang, Matthaeus, Parashar, Wu, et al., 2017; Chasapis et al., 2018; Del Sarto &

Pegoraro, 2018; Wang et al., 2019; Pezzi et al., 2019; Bandyopadhyay, Matthaeus, Parashar, et al., 2020; Matthaeus et al., 2020; Fadanelli et al., 2021; Matthaeus, 2021; Yang et al., 2022; Cassak & Barbhuiya, 2022) allows the quantification of energy conversion between the internal energy of the plasma and the bulk flow. The calculation requires multi-spacecraft velocity measurements so that the divergence and spatial gradients of the velocity field can be calculated. The method also requires measurement of the full pressure tensor. The plasma moments are derived from distribution functions comprising a finite number of measured particles. This results in the moments being affected by Poisson noise. However, an analysis of the errors associated with calculating the pressure-strain terms has not been presented.

This brief report aims to derive the equations for the error propagation for the pressure-strain terms. In the following section, we will present the Pressure-Strain methodology. The derivation of the error terms follows, and example applications to reconnection events studied by Burch et al. (2020); Lu et al. (2020); Bandyopadhyay et al. (2021) are presented.

2 Pressure-Strain methodology

The system of equations governing energy conversion in plasmas is given below. These are obtained from manipulating the Maxwell-Vlasov equations (Birn & Hesse, 2005, 2010; Cerri et al., 2016; Yang, Matthaeus, Parashar, Wu, et al., 2017; Yang, Matthaeus, Parashar, Haggerty, et al., 2017; Chasapis et al., 2018; Bandyopadhyay et al., 2021; Fadanelli et al., 2021; Matthaeus, 2021).

$$\partial_t \mathcal{E}_s^f + \nabla \cdot \left(\mathcal{E}_s^f \mathbf{V}_s + \mathbf{P}_s \cdot \mathbf{V}_s\right) = (\mathbf{P}_s \cdot \nabla) \cdot \mathbf{V}_s + n_s q_s \mathbf{E} \cdot \mathbf{V}_s \tag{1}$$

$$\partial_t \mathcal{E}_s^{in} + \nabla \cdot \left(\mathcal{E}_s^{in} \mathbf{V}_s + \mathbf{h}_s\right) = -(\mathbf{P}_s \cdot \nabla) \cdot \mathbf{V}_s \tag{2}$$

$$\partial_t \mathcal{E}^m + \frac{c}{4\pi} \nabla \cdot (\mathbf{E} \times \mathbf{B}) = -\mathbf{J} \cdot \mathbf{E} \tag{3}$$

Where, $\mathcal{E}_s^f$ is the fluid flow energy of particle species s, $\mathcal{E}^m$ is the electromagnetic energy and $\mathcal{E}_s^{in}$ is the internal (or random energy). $\mathbf{P}_s$ is the pressure tensor, $\mathbf{h}_s$ is the heat flux vector, $\mathbf{V}_s$ is the velocity, n_s is the number density, and q is the charge. Finally, $\mathbf{E}$ and $\mathbf{B}$ denote the electric and magnetic fields, and $\mathbf{J} = \sum \mathbf{J}_s$ is the total current density.

The divergence terms (on the left-hand side of Eqs. 1-3) are transport terms and move energy from one location to another. We see that the conversion of energy (right-hand side of Eqs. 1-3) can occur through different channels. The $\mathbf{J} \cdot \mathbf{E}$ term converts electromagnetic energy into kinetic energy, and the pressure-strain term converts energy between the internal energy and the bulk flow (Birn & Hesse, 2010; Del Sarto et al., 2016; Yang, Matthaeus, Parashar, Haggerty, et al., 2017; Yang, Matthaeus, Parashar, Wu, et al., 2017; Del Sarto & Pegoraro, 2018; Fadanelli et al., 2021; Matthaeus, 2021).

Energy conversion into the plasma's internal energy can only be quantified from the pressure-strain term. The pressure-strain term $(\mathbf{P}_s \cdot \nabla) \cdot \mathbf{V}_s$ therefore quantifies conversions between internal and flow energies. Calculating this quantity (due to the need for spatial gradients) requires velocity measurements at multiple points and the pressure tensor. With its four spacecraft and exceptional plasma measurements, the MMS mission is ideal for applying this methodology. The pressure-strain term can be further expressed as follows (Del Sarto et al., 2016; Yang, Matthaeus, Parashar, Haggerty, et al., 2017; Del Sarto & Pegoraro, 2018; Chasapis et al., 2018; Bandyopadhyay et al., 2021)

$$-\left(\mathbf{P}_s\cdot\nabla\right)\cdot\mathbf{V}_s=-p\delta_{ij}\partial_j u_i-\left(P_{ij}-p\delta_{ij}\right)\partial_j u_i=-p\theta-\Pi_{i,j}:D_{i,j} \tag{4}$$

where $p = \frac{1}{3}P_{i,i}$, $\theta = \nabla\cdot\mathbf{V}_s$ and $\Pi_{i,j} = P_{i,j} - p\delta_{i,j}$ is the traceless pressure tensor and $D_{ij} = \frac{1}{2}\left(\partial_i u_j + \partial_j u_i\right) - \frac{1}{3}\theta\delta_{ij}$. The delta here is the Kroenecker delta. If a plasma is incompressible, $\theta = 0$ thus, $p\theta$ denotes compressible, and ΠD denotes incompressible channels for energy conversion. By measuring these quantities with MMS, we can identify regions where energy conversion occurs. However, at the MMS separations, the differences in velocity may be very small between the spacecraft. Therefore, estimating the propagation of the uncertainty in calculating velocity gradients and the error associated with the pressure tensor is prudent.

3 Error calculation

Here we present a brief discussion of the errors in calculating the pressure-strain terms. The primary uncertainty sources come from the plasma moments and the spacecraft's positions. The spacecraft positions are known to a value < 100m, and timing accuracy across the spacecraft is < 1 ms (Tooley et al., 2016). The uncertainty from the positional and timing accuracy is negligible compared to other sources of error. The calculation of gradients will be affected if the MMS tetrahedron is irregular. Testing of the curlometer method for different constellation planarities P and elongations E (Robert, Roux, et al., 1998) demonstrated that when $\sqrt{P^2+E^2} < 0.6$ the error on the current estimation was $< 3\%$ and $\sqrt{P^2+E^2} \sim 0.9$ the error was of the order of 10% (Robert, Dunlop, et al., 1998). However, suppose the tetrahedron is regular, and the positions are well known. In that case, the uncertainty due to the spacecraft positions is expected to be small compared to the errors on the plasma moments.

The other source of error comes from the plasma moments themselves. Plasma instruments count individual particles; consequently, there will be random errors due to Poisson noise (i.e., related to the counting statistics). The statistical errors on the moments from MMS are available in the Fast Plasma Investigation (FPI) (Pollock et al., 2016) level-2 moments. Note level-2 means the science quality, ground processed moments, where corrections becuase of the spacecraft potential have been applied. Details of the calculation of the statistical errors are available in Gershman et al. (2015). They are based on error propagation and consider the counts in the instrument (instrument true response), and the phase space density (calibrated instrument response).

The divergence uncertainty was investigated by Vogt and Paschmann (1998). The calculation of a divergence from four point measurements is given by;

$$\nabla\cdot\boldsymbol{V}\simeq\sum_{\alpha}\boldsymbol{k}_\alpha\cdot\boldsymbol{V}_\alpha \tag{5}$$

where α denotes the spacecraft $\boldsymbol{k}$ is the reciprocal vector defined as;

$$\boldsymbol{k}_\alpha=\frac{\boldsymbol{r}_{\beta\gamma}\times\boldsymbol{r}_{\beta\lambda}}{\boldsymbol{r}_{\beta\alpha}\cdot\left(\boldsymbol{r}_{\beta\gamma}\times\boldsymbol{r}_{\beta\lambda}\right)} \tag{6}$$

where $\boldsymbol{r}_{\alpha,\beta} = \boldsymbol{r}_\beta - \boldsymbol{r}_\alpha$ are the relative position vectors of the four spacecraft, where $(\alpha,\beta,\gamma,\lambda)$ must be a cyclic permutation of (1,2,3,4) (Chanteur, 1998; Vogt, Paschmann, & Chanteur, 2008).

Suppose the tetrahedron is close to a regular and the spacecraft positions are well known. In that case, we can neglect the error on the reciprocal vectors and only consider the error on the plasma measurements. The error on the divergence of velocity derived in Vogt and Paschmann (1998) is then given by:

$$\sigma[\nabla \cdot \mathbf{V}] \simeq \sqrt{\sum_{\alpha} \left(\mathbf{k}_{\alpha}^2 \cdot \sigma \left[\mathbf{V}_{\alpha} \right]^2 \right)}. \quad (7)$$

Here σ denotes the error of the quantity in the square brackets. Therefore the error on the compressive part of the pressure-strain term comes from a combination of the error from Eq. 7 and the error on the pressure tensor $\mathbf{P}_{\mathrm{Error}}$. We use the equations for uncertainty propagation to estimate the combined error. We averaged the pressure tensors from the four spacecraft

$$\mathbf{P}_{\mathrm{av}} = \frac{1}{4} \sum_{\alpha} \mathbf{P}_{\alpha}, \quad (8)$$

the associated errors on the pressure tensor are propagated following;

$$\mathbf{P}_{\mathrm{av,Error}} = \frac{1}{4} \sqrt{\mathbf{P}_{1,\mathrm{err}}^2 + \mathbf{P}_{2,\mathrm{err}}^2 + \mathbf{P}_{3,\mathrm{err}}^2 + \mathbf{P}_{4,\mathrm{err}}^2}, \quad (9)$$

the total pressure is given by:

$$p = \frac{1}{3} \sum_{i} \mathbf{P}_{\mathrm{av},ii}, \quad (10)$$

and the corresponding error is:

$$\sigma[p] = \frac{1}{3} \sqrt{P_{\mathrm{av,Error},11}^2 + P_{\mathrm{av,Error},22}^2 + P_{\mathrm{av,Error},33}^2}. \quad (11)$$

The final error on the $p\theta$ term is given by:

$$\sigma[p\theta] = |p\theta| \sqrt{\left(\frac{\sigma[\nabla \cdot \boldsymbol{V}]}{\nabla \cdot \boldsymbol{V}} \right)^2 + \left(\frac{\sigma[p]}{p} \right)^2}. \quad (12)$$

For the calculation of a directional derivative (in the direction x_i), the errors are given by:

$$\sigma \left[\frac{\partial V_j}{\partial x_i} \right] = \sqrt{\sum_{\alpha} \left(k_{\alpha i}^2 \sigma \left[V_{\alpha,j} \right]^2 \right)}. \quad (13)$$

The errors on the D term then become;

$$D_{ij,\mathrm{Error}} = \frac{1}{2} \sqrt{\left(\sigma \left[\frac{\partial V_j}{\partial x_i} \right]^2 + \sigma \left[\frac{\partial V_i}{\partial x_j} \right]^2 \right)}. \quad (14)$$

Note that D_{ij} is defined as ;

$$D_{ij} = \frac{1}{2} \left(\partial_i V_j + \partial_j V_i \right) - \frac{1}{3} \theta \delta_{ij} \quad (15)$$

therefore there would be some additional error due to the divergence term $\frac{1}{3}\theta\delta_{ij}$ for the diagonals. However, this contribution can be ignored as this matrix combines the traceless pressure tensor $\Pi_{i,j}$ (where the diagonal elements are zero) through the tensor double contraction.

Combining the errors from the traceless pressure tensor and D we obtain a combined error tensor.

$$\sigma\left[D_{i,j}\Pi_{i,j}\right] = |D_{ij}\Pi_{ij}|\sqrt{\left(\frac{D_{i,j,Error}}{D_{i,j}}\right)^2 + \left(\frac{\Pi_{Error,i,j}}{\Pi_{i,j}}\right)^2} \tag{16}$$

Only three unique error terms exist in Eq 16 because the D and the Π tensors (and their errors) are symmetric i.e. $\sigma\left[D_{0,1}\Pi_{0,1}\right] = \sigma\left[D_{1,0}\Pi_{1,0}\right]$. This effectively means we must consider the error on a diagonal term, double it, and propagate it (as the error on an element appears twice in the double contraction). Thus, the final error on the ΠD term is then given by:

$$\sigma[\Pi D] = 2\sqrt{\sigma\left[D_{0,1}\Pi_{0,1}\right]^2 + \sigma\left[D_{0,2}\Pi_{0,2}\right]^2 + \sigma\left[D_{1,2}\Pi_{1,2}\right]^2} \tag{17}$$

For completeness, the total pressure-strain term error is given in 18.

$$\sigma_{(\mathbf{P}_s\cdot\nabla)\cdot\mathbf{V}_s} = \sqrt{\sigma[p\theta]^2 + \sigma[\Pi D]^2} \tag{18}$$

4 Application to the Terrestrial magnetosphere

Two examples of the application of the method and the error calculation are now presented. The data are from MMS when the spacecraft were in the burst telemetry mode; magnetic field data are from the fluxgate magnetometers (Russell et al., 2016) with a sampling rate of 128 Hz. The plasma data are from the FPI instrument (Pollock et al., 2016), where the sampling rates are 6.6 Hz for ions and 30.3 Hz for electrons. Figure 1 show an example of magnetic reconnection studied by Burch et al. (2020) and later using the pressure-strain methodology by Bandyopadhyay et al. (2021). MMS was at the magnetopause in this case, and the mean electron number density was moderate 7.19 cm^{-3}. The spacecraft constellation $\sqrt{P^2+E^2} = 0.62$ was not perfectly regular but was enough that the error on the reciprocal vectors is expected to be small (less than 3% Robert, Dunlop, et al. (1998)). To calculate the pressure-strain terms, we remove the spin effects using the spin tone product in the FPI L2 data files before calculating the gradients. We see that the errors are small, and the application of the method is justified.

Figure 2 presents a second magnetic reconnection case. This case studied previously by Lu et al. (2020) occurs in the magnetotail. Magnetotail plasma is typically much more tenuous compared to magnetosheath/magnetopause plasma. In this case, the mean electron number density is 0.58 cm^{-3}; therefore, we expect the errors to be larger due to poor counting statistics. For this case the spacecraft constellation $\sqrt{P^2+E^2} = 0.35$. The absolute errors for both cases are given in Tab 1. As expected, the absolute errors in the magnetotail are significantly larger than at the magnetopause.

We perform a statistical Monte Carlo test on the data to provide an additional estimate of the error. We take the individual velocity and pressure tensor series and their respective errors and compute 100 new time series. This is performed by adding a random (Gaussian distributed) error with a mean of zero and a standard deviation equal to the statistical error to the measured velocity and pressure tensor components. We perform this procedure one hundred times and calculate the pressure strain terms with each of our realizations of the time series. We calculate the standard deviation from the 100 realizations for each point, yielding another error estimate. This analysis is presented in Figs 3,4. The standard deviation of the one hundred time series agrees well with those

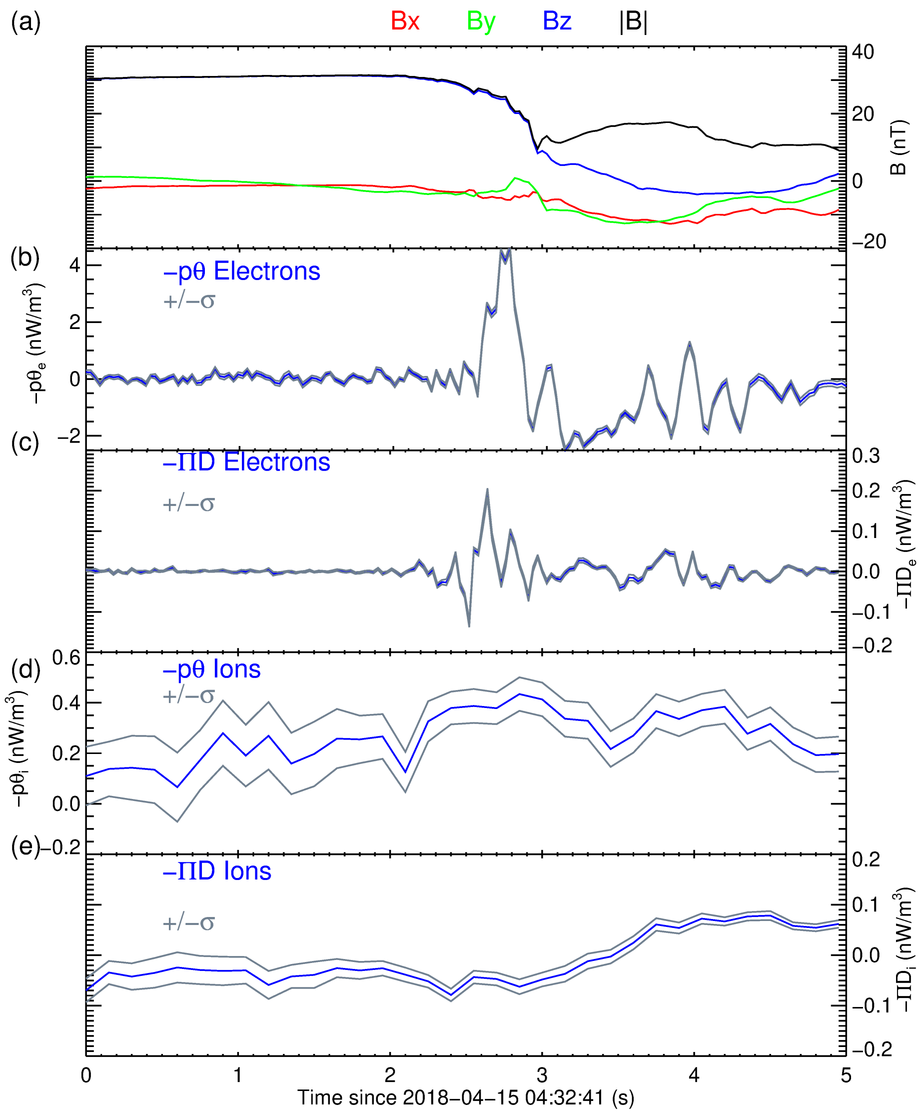

Figure 1. MMS measurements taken during the magnetopause magnetic reconnection event of Burch et al. (2020).(a) Magnetic field measurements from the fluxgate magnetometer in the Geocentric Solar Ecliptic coordinate system. (b) the compressive electron component of the pressure-strain term (c) the incompressible electron component of the pressure-strain term (d) the ion compressive component of the pressure-strain term, and (e) the ion incompressive component. In panels (b-e) blue denotes the measurement, and grey denotes three times the estimated error.

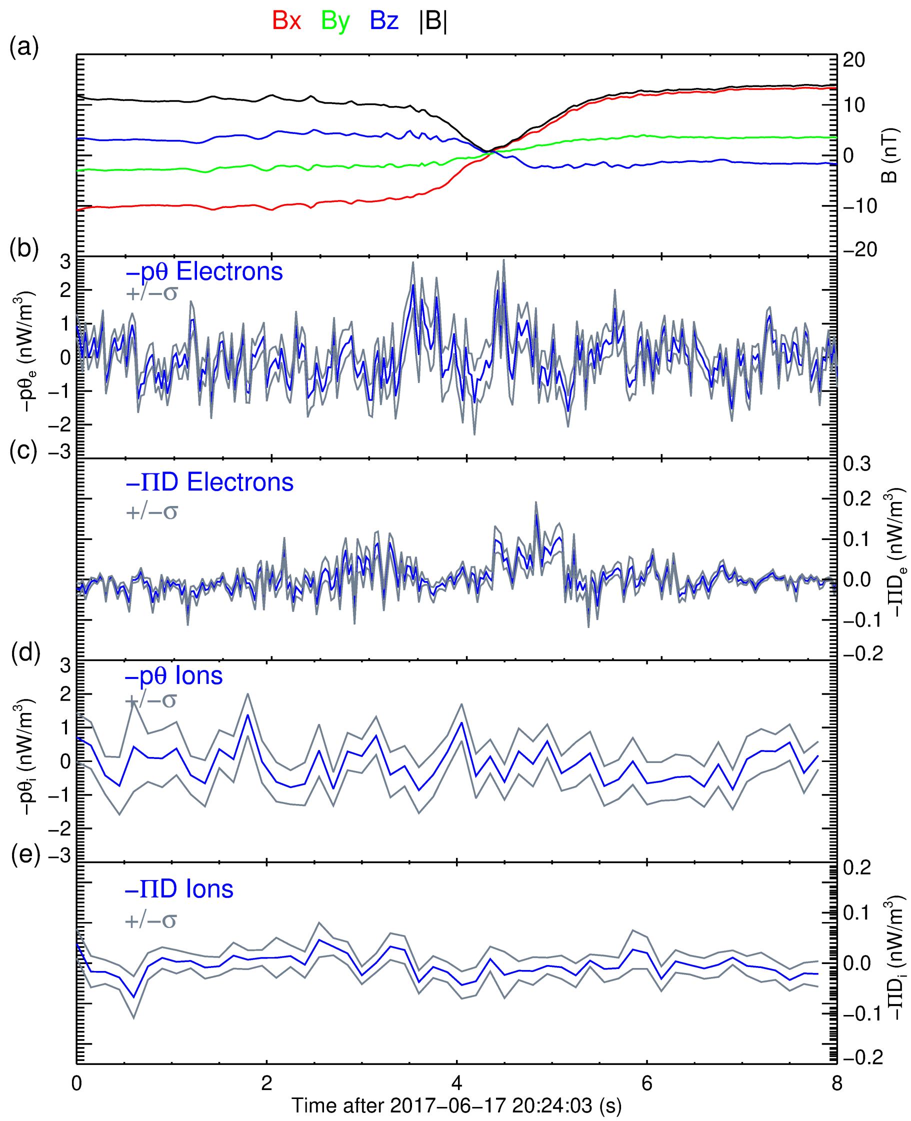

Figure 2. The same as Fig 1 but for the magnetotail event of (Lu et al., 2020).

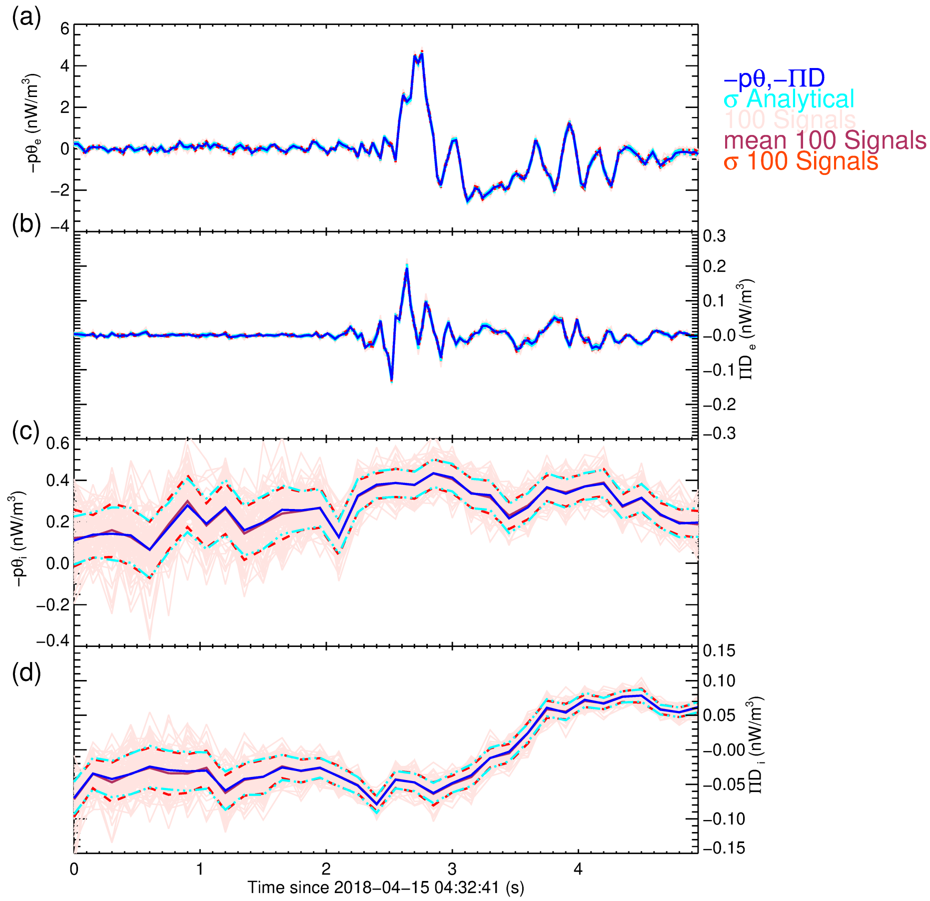

Figure 3. The different electron and ion pressure strain terms for the magnetopause event. Blue denotes the pressure strain terms, and cyan denotes the analytical error. The pink lines denote 100 time series where a random error is introduced (see text), the maroon denotes the mean of these time series (almost identical to the blue curve). The red lines denote the standard deviation of these 100 time series giving an additional estimation of the error, which agrees well with the cyan curves.

estimated through the equations given in the previous section, giving further confidence in the error estimation and the technique itself.

To better understand the limitations of the method in different regions that MMS surveys, we plot the electron number density (Figure 5a) and the relative errors on the ion (Figure 5b) and electron bulk speeds (Figure 5c) as a function of the spacecraft position in the xy GSE plane in the year 2018. Here we see that the errors are significantly larger in the magnetotail where the density is lower. The relative errors on the electron bulk velocities are also larger than those of the ions; this is possibly due to the effects of photoelectrons (Lavraud & Larson, 2016; Gershman et al., 2017), which are removed using a model from the L2 data, which may cause larger uncertainties, especially when counts are already low. Therefore we would urge caution when using the method in low-density regions.

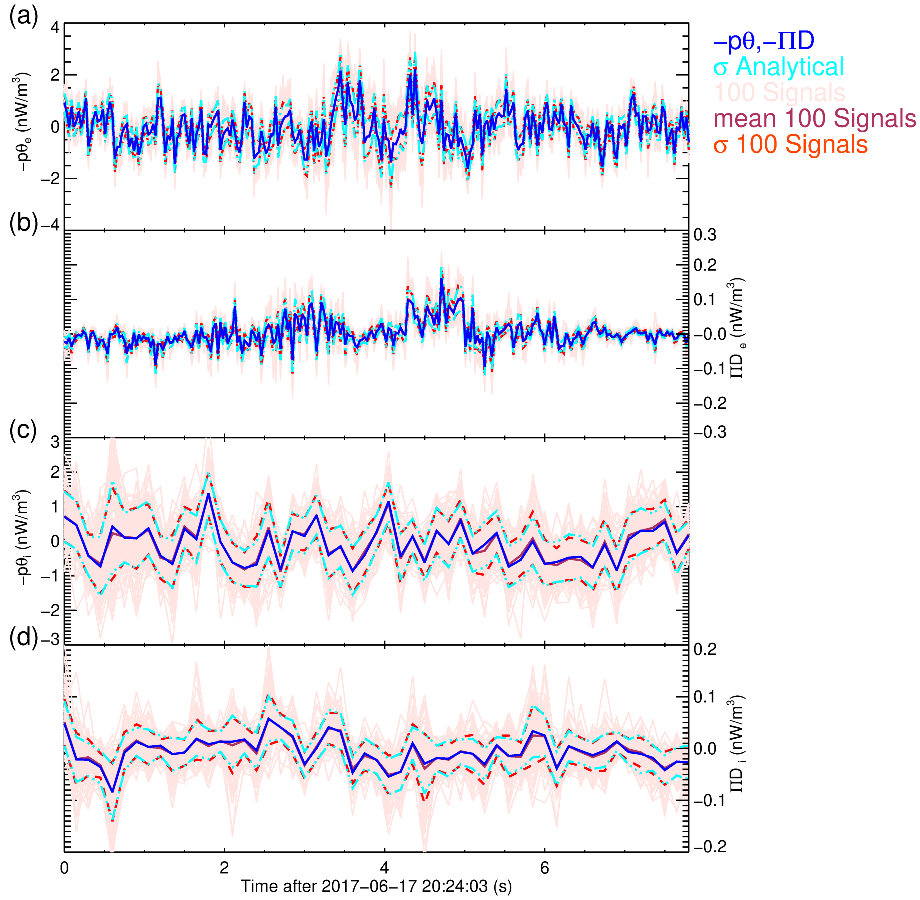

Figure 4. Same as Figure 3 but for the magnetotail case.

Table 1. Table of the absolute errors for both cases studied. Note that the $p\theta$ and ΠD fluctuate quantities around zero, so we do not state the relative error as this may be undefined when the measured quantity is zero.

	Electrons		Ions	
	$\sigma[p\theta]$ (nW/m^3)	$\sigma[\Pi D]$ (nW/m^3)	$\sigma[p\theta]$ (nW/m^3)	$\sigma[\Pi D]$ (nW/m^3)
Magnetopause ($n = 7.19$ cm^{-3})				
Analytical	0.087	0.004	0.089	0.017
Resampling method	0.087	0.004	0.089	0.017
Magnetotail ($n = 0.58$ cm^{-3})				
Analytical	0.425	0.016	0.632	0.030
Resampling method	0.426	0.017	0.628	0.033

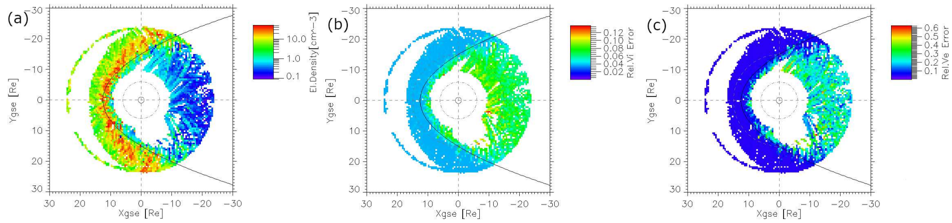

Figure 5. MMS fast survey mode data from 2018 as a function of the spacecraft position in the xy GSE plane. (a) shows the electron density measured by FPI. (b) and (c) show the relative error in the bulk velocity for ions and electrons, respectively.

5 Summary

To summarize, we have investigated the uncertainties in the pressure strain terms through error propagation and a statistical test. Both approaches yield almost identical results. Relations have been given to estimate the error. The error here is assumed mostly due to Poisson noise in the plasma moments. We did not investigate the uncertainty due to the spacecraft positions (which are expected to be small) or the uncertainty due to an inhomogeneous tetrahedron (which can be mitigated with appropriate event selection). Furthermore, there could be other errors, which we will briefly discuss.

Because of instrument design, there can be an offset in a velocity component between spacecraft; for MMS, this most likely affects the V_z component. This systematic error could cause an additional error in the gradient measurements. Another possible source of error is related to the spacecraft separations; by calculating a gradient using multiple spacecraft, we are looking at a spatial gradient accurate to a certain scale. Different plasma species have different length scales, so spacecraft separations may be inadequate for measuring the pressure strain interaction for a certain species. Numerical simulations by Matthaeus et al. (2020) and Yang et al. (2022) show scale dependence in the average value of the pressure strain term. At inertial scales, the average of the pressure strain term is small but increases at length scales below the ion inertial length. Thus the relative error at different scales may differ even if the statistical errors on the moments are equal. With MMS, we are limited to electron scale separations where the pressure strain terms are expected to be large. However, comparisons with numerical simulations, or spacecraft data with multiple separations (relative to the ion/electron characteristic scales) would be useful to understand how the spacecraft separations may affect the result (Bandyopadhyay, Matthaeus, Parashar, et al., 2020). This would be especially useful in preparation for HelioSwarm as the nine spacecraft allow multi-scale estimations of the pressure strain terms. Other potential sources of error may come from the calibration, penetrating radiation, spin tones, and effects due to spacecraft charging.

Two examples in different plasma conditions were presented; the propagated errors at the magnetopause were smaller than the tail, as expected, due to lower counting statistics in the tail. While the errors are generally small, caution should be exercised in low plasma regions, where counting statistics are poor. However, we expect calculating the pressure strain terms in the magnetosheath (high density) to have an excellent signal-to-noise ratio. It should, however, be noted that FPI is not designed for the solar wind and is subject to substantial variations at the spacecraft spin frequency (Bandyopadhyay et al., 2018; O. W. Roberts et al., 2021; Wilson III et al., 2022); this method should not be used with MMS in the solar wind.

.

Acknowledgments

The datasets analyzed for this study can be found in the MMS data archive `https://lasp.colorado.edu/mms/sdc/public/`. OWR gratefully acknowledges the Austrian Science Fund (FWF): P 33285-N for supporting this project. We acknowledge the fluxgate magnetometer and the fast plasma investigation teams for the excellent data MMS provides that makes using such techniques possible. This research was supported by the International Space Science Institute (ISSI) in Bern, through ISSI International Team project #556 (Cross-scale energy transfer in space plasmas).

References

Angelopoulos, V. (2008, dec). The THEMIS Mission. *Space Science Reviews*, *141*(1-4), 5–34. doi: 10.1007/s11214-008-9336-1

Bandyopadhyay, R., Chasapis, A., Chhiber, R., Parashar, T. N., Maruca, B. A., Matthaeus, W. H., … Strangeway, R. J. (2018, oct). Solar Wind Turbulence Studies Using MMS Fast Plasma Investigation Data. *The Astrophysical Journal*, *866*(2), 81. doi: 10.3847/1538-4357/aade93

Bandyopadhyay, R., Chasapis, A., Matthaeus, W. H., Parashar, T. N., Haggerty, C. C., Shay, M. A., … Burch, J. L. (2021). Energy dissipation in turbulent reconnection. *Physics of Plasmas*, *28*(11). doi: 10.1063/5.0071015

Bandyopadhyay, R., Matthaeus, W. H., Chasapis, A., Russell, C. T., Strangeway, R. J., Torbert, R. B., … Burch, J. L. (2020, aug). Direct Measurement of the Solar-wind Taylor Microscale Using MMS Turbulence Campaign Data. *The Astrophysical Journal*, *899*(1), 63. doi: 10.3847/1538-4357/ab9ebe

Bandyopadhyay, R., Matthaeus, W. H., Parashar, T. N., Yang, Y., Chasapis, A., Giles, B. L., … Burch, J. L. (2020). Statistics of Kinetic Dissipation in the Earth's Magnetosheath: MMS Observations. *Physical Review Letters*, *124*(25). doi: 10.1103/PhysRevLett.124.255101

Birn, J., & Hesse, M. (2005). Energy release and conversion by reconnection in the magnetotail. *Annales Geophysicae*, *23*(10), 3365–3373. doi: 10.5194/angeo-23-3365-2005

Birn, J., & Hesse, M. (2010, jan). Energy release and transfer in guide field reconnection. *Physics of Plasmas*, *17*(1), 012109. doi: 10.1063/1.3299388

Broeren, T., Klein, K. G., TenBarge, J. M., Dors, I., Roberts, O. W., & Verscharen, D. (2021, sep). Magnetic Field Reconstruction for a Realistic Multi-Point, Multi-Scale Spacecraft Observatory. *Frontiers in Astronomy and Space Sciences*, *8*. doi: 10.3389/fspas.2021.727076

Burch, J. L., Moore, T. E., Torbert, R. B., & Giles, B. L. (2016, mar). Magnetospheric Multiscale Overview and Science Objectives. *Space Science Reviews*, *199*(1-4), 5–21. doi: 10.1007/s11214-015-0164-9

Burch, J. L., Webster, J. M., Hesse, M., Genestreti, K. J., Denton, R. E., Phan, T. D., … Paschmann, G. (2020). Electron Inflow Velocities and Reconnection Rates at Earth's Magnetopause and Magnetosheath. *Geophysical Research Letters*, *47*(17), 1–10. doi: 10.1029/2020GL089082

Cassak, P. A., & Barbhuiya, M. H. (2022, dec). Pressure–strain interaction. I. On compression, deformation, and implications for Pi-D. *Physics of Plasmas*, *29*(12), 122306. doi: 10.1063/5.0125248

Cerri, S. S., Califano, F., Jenko, F., Told, D., & Rincon, F. (2016). Subproton-Scale Cascades in Solar Wind Turbulence: Driven Hybrid-Kinetic Simulations. *The Astrophysical Journal*, *822*(1), L12. doi: 10.3847/2041-8205/822/1/L12

Chanteur, G. (1998). Spatial Interpolation for Four Spacecraft: Theory. In *Analysis methods for multi-spacecraft data* (chap. 14). ISSI.

Chasapis, A., Yang, Y., Matthaeus, W. H., Parashar, T. N., Haggerty, C. C., Burch, J. L., … Russell, C. T. (2018). Energy Conversion and Collisionless Plasma Dissipation Channels in the Turbulent Magnetosheath Observed by the Magnetospheric Multiscale Mission. *The Astrophysical Journal*, *862*(1), 32. doi: 10.3847/1538-4357/aac775

Chen, C. H. K., Horbury, T. S., Schekochihin, A. A., Wicks, R. T., Alexandrova, O., & Mitchell, J. (2010, jun). Anisotropy of Solar Wind Turbulence between Ion and Electron Scales. *Physical Review Letters*, *104*(255002), 1–4. doi: 10.1103/PhysRevLett.104.255002

Constantinescu, O. (2007). *Wave Sources and Structures in the Earth's Magnetosheath and Adjacent Regions* (Doctoral dissertation).

Del Sarto, D., & Pegoraro, F. (2018, mar). Shear-induced pressure anisotropization and correlation with fluid vorticity in a low collisionality plasma. *Monthly Notices of the Royal Astronomical Society*, *475*(1), 181–192. doi: 10.1093/mnras/stx3083

Del Sarto, D., Pegoraro, F., & Califano, F. (2016). Pressure anisotropy and small spatial scales induced by velocity shear. *Physical Review E*, *93*(5). doi: 10.1103/PhysRevE.93.053203

Denton, R. E., Liu, Y., Hasegawa, H., Torbert, R. B., Li, W., Fuselier, S., & Burch, J. L. (2022, oct). Polynomial Reconstruction of the Magnetic Field Observed by Multiple Spacecraft With Integrated Velocity Determination. *Journal of Geophysical Research: Space Physics*, *127*(10). doi: 10.1029/2022JA030512

Denton, R. E., Torbert, R. B., Hasegawa, H., Dors, I., Genestreti, K. J., Argall, M. R., ... Fischer, D. (2020). Polynomial Reconstruction of the Reconnection Magnetic Field Observed by Multiple Spacecraft. *Journal of Geophysical Research: Space Physics*, *125*(2), 1–52. doi: 10.1029/2019ja027481

Dudok de Wit, T., Bale, S., Krasnosel'skikh, V. V., Dunlop, M. W., Lühr, H., Woolliscroft, L. J. C., & Schwartz, S. J. (1995). Determination of dispersion relations in quasi-stationary plasma turbulence using dual satellite data. *Geophysical Research Letters*, *22*(19), 2653.

Dunlop, M., Southwood, D., Glassmeier, K.-H., & Neubauer, F. (1988, jan). Analysis of multipoint magnetometer data. *Advances in Space Research*, *8*(9-10), 273–277. doi: 10.1016/0273-1177(88)90141-X

Dunlop, M. W., Balogh, A., Glassmeier, K.-H., & Robert, P. (2002). Four-point Cluster application of magnetic field analysis tools: The Curlometer. *Journal of Geophysical Research: Space Physics*, *107*(A11), 1–14. doi: 10.1029/2001JA005088

Dunlop, M. W., Dong, X. C., Wang, T. Y., Eastwood, J. P., Robert, P., Haaland, S., ... De Keyser, J. (2021). Curlometer Technique and Applications. *Journal of Geophysical Research: Space Physics*, *126*(11). doi: 10.1029/2021JA029538

Escoubet, C. P., Fehringer, M., & Goldstein, M. (2001). Introduction The Cluster mission. *Annales Geophysicae*, *19*, 1197–1200. doi: 10.5194/angeo-19-1197-2001

Escoubet, C. P., Schmidt, R., & Goldstein, M. (1997). CLUSTER – SCIENCE AND MISSION OVERVIEW. *Space Science Reviews*, *79*(1-2), 11–32.

Fadanelli, S., Lavraud, B., Califano, F., Cozzani, G., Finelli, F., & Sisti, M. (2021). Energy Conversions Associated With Magnetic Reconnection. *Journal of Geophysical Research: Space Physics*, *126*(1), 1–12. doi: 10.1029/2020JA028333

Friis-Christensen, E., Lühr, H., Knudsen, D., & Haagmans, R. (2008, jan). Swarm – An Earth Observation Mission investigating Geospace. *Advances in Space Research*, *41*(1), 210–216. doi: 10.1016/j.asr.2006.10.008

Gershman, D. J., Avanov, L. A., Boardsen, S. A., Dorelli, J. C., Gliese, U., Barrie, A. C., ... Pollock, C. J. (2017, nov). Spacecraft and Instrument Photoelectrons Measured by the Dual Electron Spectrometers on MMS. *Journal of Geophysical Research: Space Physics*, *122*(11), 11,548–11,558. doi: 10.1002/2017JA024518

Gershman, D. J., Dorelli, J. C., F.-Viñas, A., & Pollock, C. J. (2015, aug). The calculation of moment uncertainties from velocity distribution functions with random errors. *Journal of Geophysical Research: Space Physics*, *120*(8), 6633–6645. doi: 10.1002/2014JA020775

Gershman, D. J., F.-Viñas, A., Dorelli, J. C., Goldstein, M. L., Shuster, J., Avanov, L. A., ... Burch, J. L. (2018, feb). Energy partitioning constraints at kinetic scales in low- β turbulence. *Physics of Plasmas*, *25*(2), 022303. doi: 10.1063/1.5009158

Glassmeier, K.-H., Motschmann, U., Dunlop, M., Balogh, A., Acuña, M. H., Carr, C., ... Buchert, S. (2001, sep). Cluster as a wave telescope – first results from the fluxgate magnetometer. *Annales Geophysicae*, *19*(10/12), 1439–1447. doi: 10.5194/angeo-19-1439-2001

Horbury, T. (2000). Cluster II analysis of turbulence using correlation functions. In *Cluster-ii workshop: Multiscale/multipoint plasma measurements* (pp. 89–97).

Kieokaew, R., & Foullon, C. (2019). Kelvin-Helmholtz Waves Magnetic Curvature and Vorticity: Four-Spacecraft Cluster Observations. *Journal of Geophysical Research: Space Physics*, *124*(5), 3347–3359. doi: 10.1029/2019JA026484

Klein, K. G., Alexandrova, O., Bookbinder, J., Caprioli, D., Case, A. W., Chandran, B. D. G., ... Whittlesey, P. (2019, mar). [Plasma 2020 Decadal] Multipoint Measurements of the Solar Wind: A Proposed Advance for Studying Magnetized Turbulence.
doi: arXiv:1903.05740

Lavraud, B., & Larson, D. E. (2016, sep). Correcting moments of in situ particle distribution functions for spacecraft electrostatic charging. *Journal of Geophysical Research: Space Physics*, *121*(9), 8462–8474. doi: 10.1002/2016JA022591

Lavraud, B., Zhang, Y. C., Vernisse, Y., Gershman, D. J., Dorelli, J., Cassak, P. A., ... Yokota, S. (2016). Currents and associated electron scattering and bouncing near the diffusion region at Earth's magnetopause. *Geophysical Research Letters*, *43*(7), 3042–3050. doi: 10.1002/2016GL068359

Lu, S., Wang, R., Lu, Q., Angelopoulos, V., Nakamura, R., Artemyev, A. V., ... Wang, S. (2020). Magnetotail reconnection onset caused by electron kinetics with a strong external driver. *Nature Communications*, *11*(1), 1–7. doi: 10.1038/s41467-020-18787-w

Matthaeus, W. H. (2021). Turbulence in space plasmas: Who needs it? *Physics of Plasmas*, *28*(3). doi: 10.1063/5.0041540

Matthaeus, W. H., Dasso, S., Weygand, J. M., Milano, L. J., Smith, C. W., & Kivelson, M. G. (2005, dec). Spatial Correlation of Solar-Wind Turbulence from Two-Point Measurements. *Physical Review Letters*, *95*(23), 231101. doi: 10.1103/PhysRevLett.95.231101

Matthaeus, W. H., Yang, Y., Wan, M., Parashar, T. N., Bandyopadhyay, R., Chasapis, A., ... Valentini, F. (2020). Pathways to Dissipation in Weakly Collisional Plasmas. *The Astrophysical Journal*, *891*(1), 101. doi: 10.3847/1538-4357/ab6d6a

Motschmann, U., Woodward, T. I., Glassmeier, K. H., Southwood, D. J., & Pinçon, J. L. (1996, mar). Wavelength and direction filtering by magnetic measurements at satellite arrays: Generalized minimum variance analysis. *Journal of Geophysical Research: Space Physics*, *101*(A3), 4961–4965. doi: 10.1029/95JA03471

Narita, Y., Glassmeier, K.-H., & Motschmann, U. (2010, sep). Wave vector analysis methods using multi-point measurements. *Nonlinear Processes in Geophysics*, *17*(5), 383–394. doi: 10.5194/npg-17-383-2010

Narita, Y., Glassmeier, K.-H., & Motschmann, U. (2011, feb). High-resolution wave number spectrum using multi-point measurements in space – the Multi-point Signal Resonator (MSR) technique. *Annales Geophysicae*, *29*(2), 351–360. doi: 10.5194/angeo-29-351-2011

Narita, Y., Plaschke, F., & Vörös, Z. (2021, apr). The Magnetosheath. In (pp. 137–152). doi: 10.1002/9781119815624.ch9

Osman, K., & Horbury, T. (2009, jun). Quantitative estimates of the slab and 2-D power in solar wind turbulence using multispacecraft data. *Journal of Geophysical Research*, *114*(A06103), 1–8. doi: 10.1029/2008JA014036

Osman, K. T., & Horbury, T. S. (2007, jan). Multispacecraft Measurement of Anisotropic Correlation Functions in Solar Wind Turbulence. *The Astrophysical Journal*, *654*(1), L103–L106. doi: 10.1086/510906

Paschmann, G. (1998). *Analysis Methods for Multi-Spacecraft Data* (G. Paschmann, Ed.).

Paschmann, G., & Daly, P. (2008). *Multi-spacecraft analysis methods revisited*.

Pecora, F., Servidio, S., Primavera, L., Greco, A., Yang, Y., & Matthaeus, W. H. (2023, mar). Multipoint Turbulence Analysis with HelioSwarm. *The Astrophysical Journal Letters*, *945*(2), L20. doi: 10.3847/2041-8213/acbb03

Perri, S., Valentini, F., Sorriso-Valvo, L., Reda, A., & Malara, F. (2017, jun). On the estimation of the current density in space plasmas: Multi- versus single-point techniques. *Planetary and Space Science*, *140*(November 2016), 6–10. doi: 10.1016/j.pss.2017.03.008

Perrone, D., Alexandrova, O., Mangeney, A., Maksimovic, M., Lacombe, C., Rakoto, V., … Jovanovic, D. (2016, jul). COMPRESSIVE COHERENT STRUCTURES AT ION SCALES IN THE SLOW SOLAR WIND. *The Astrophysical Journal*, *826*(2), 196. doi: 10.3847/0004-637X/826/2/196

Perrone, D., Alexandrova, O., Roberts, O. W., Lion, S., Lacombe, C., Walsh, A., … Zouganelis, I. (2017, oct). Coherent Structures at Ion Scales in Fast Solar Wind: Cluster Observations. *The Astrophysical Journal*, *849*(1), 49. doi: 10.3847/1538-4357/aa9022

Pezzi, O., Yang, Y., Valentini, F., Servidio, S., Chasapis, A., Matthaeus, W. H., & Veltri, P. (2019). Energy conversion in turbulent weakly collisional plasmas: Eulerian hybrid Vlasov-Maxwell simulations. *Physics of Plasmas*, *26*(7), 1–11. doi: 10.1063/1.5100125

Phan, T. D., Eastwood, J. P., Cassak, P. A., Øieroset, M., Gosling, J. T., Gershman, D. J., … Wilder, F. D. (2016). MMS observations of electron-scale filamentary currents in the reconnection exhaust and near the X line. *Geophysical Research Letters*, *43*(12), 6060–6069. doi: 10.1002/2016GL069212

Pincon, J., & Lefeuvre, F. (1991). Local characterization of homogeneous turbulence in a space plasma from simultaneous measurements of field components at several points in space. *Journal of Geophysical Research*, *96*(A2), 1789–1802.

Pollock, C., Moore, T., Jacques, A., Burch, J., Gliese, U., Saito, Y., … Zeuch, M. (2016, mar). Fast Plasma Investigation for Magnetospheric Multiscale. *Space Science Reviews*, *199*(1-4), 331–406. doi: 10.1007/s11214-016-0245-4

Robert, P., Dunlop, M. W., Roux, A., & Chanteur, G. (1998). Accuracy of Current Density Determination. *Analysis Methods for Multi-Spacecraft Data*, *001*, 395–418.

Robert, P., Roux, A., Harvey, C., Dunlop, M., Daly, P., & Glassmeier, K.-H. (1998). Tetrahedron Geometric Factors. In P. Paschmann, G Daly (Ed.), *Analysis methods for multi-spacecraft data* (pp. 323–348).

Roberts, O., Li, X., & Jeska, L. (2014). Validation of the k-filtering technique for a signal composed of random phase plane waves and non-random coherent structures. *Geoscientific Information and Data Systems*, *3*, 247–254. doi: doi:10.5194/gi-3-247-2014

Roberts, O. W., Alexandrova, O., Sorriso-Valvo, L., Vörös, Z., Nakamura, R., Fischer, D., … Yearby, K. (2022, sep). Scale-Dependent Kurtosis of Magnetic Field Fluctuations in the Solar Wind: A Multi-Scale Study With Cluster 2003–2015. *Journal of Geophysical Research: Space Physics*, *127*(9), 1–25. doi: 10.1029/2021JA029483

Roberts, O. W., Nakamura, R., Coffey, V. N., Gershman, D. J., Volwerk, M., Varsani, A., … Pollock, C. (2021). A Study of the Solar Wind Ion and Electron Measurements From the Magnetospheric Multiscale Mission's Fast Plasma Investigation. *Journal of Geophysical Research: Space Physics*, *126*(10), 1–18. doi: 10.1029/2021ja029784

Roberts, O. W., Narita, Y., Li, X., Escoubet, C. P., & Laakso, H. (2017, jul). Multipoint analysis of compressive fluctuations in the fast and slow solar wind. *Journal of Geophysical Research: Space Physics*, *122*(7), 6940–6963. doi: 10.1002/2016JA023552

Russell, C. T., Anderson, B. J., Baumjohann, W., Bromund, K. R., Dearborn, D., Fischer, D., ... Richter, I. (2016). The Magnetospheric Multiscale Magnetometers. *Space Science Reviews*, *199*(1-4), 189–256. doi: 10.1007/s11214-014-0057-3

Tooley, C. R., Black, R. K., Robertson, B. P., Stone, J. M., Pope, S. E., & Davis, G. T. (2016). The Magnetospheric Multiscale Constellation. *Space Science Reviews*, *199*(1-4), 23–76. doi: 10.1007/s11214-015-0220-5

Vogt, J., Narita, Y., & Constantinescu, O. (2008). The wave surveyor technique for fast plasma wave detection in multi-spacecraft data. *Annales Geophysicae*, 1699–1710.

Vogt, J., & Paschmann, G. (1998). Accuracy of Plasma Moment Derivatives. In G. Paschmann & P. Daly (Eds.), *Analysis methods for multi-spacecraft data* (chap. 17). ISSI.

Vogt, J., Paschmann, G., & Chanteur, G. (2008). Reciprocal Vectors. In G. Paschmann & P. Daly (Eds.), *Multi-spacecraft analysis methods revisited.* ISSI.

Wang, T., Alexandrova, O., Perrone, D., Dunlop, M., Dong, X., Bingham, R., ... Burch, J. L. (2019). Magnetospheric Multiscale Observation of Kinetic Signatures in the Alfvén Vortex. *The Astrophysical Journal*, *871*(2), L22. doi: 10.3847/2041-8213/aafe0d

Wilson III, L. B., Goodrich, K. A., Turner, D. L., Cohen, I. J., Whittlesey, P. L., & Schwartz, S. J. (2022). The need for accurate measurements of thermal velocity distribution functions in the solar wind. *Frontiers in Astronomy and Space Sciences*, *9*(November). doi: 10.3389/fspas.2022.1063841

Yang, Y., Matthaeus, W. H., Parashar, T. N., Haggerty, C. C., Roytershteyn, V., Daughton, W., ... Chen, S. (2017, jul). Energy transfer, pressure tensor, and heating of kinetic plasma. *Physics of Plasmas*, *24*(7), 072306. doi: 10.1063/1.4990421

Yang, Y., Matthaeus, W. H., Parashar, T. N., Wu, P., Wan, M., Shi, Y., ... Daughton, W. (2017). Energy transfer channels and turbulence cascade in Vlasov-Maxwell turbulence. *Physical Review E*, *95*(6). doi: 10.1103/PhysRevE.95.061201

Yang, Y., Matthaeus, W. H., Roy, S., Roytershteyn, V., Parashar, T. N., Bandyopadhyay, R., & Wan, M. (2022). Pressure–Strain Interaction as the Energy Dissipation Estimate in Collisionless Plasma. *The Astrophysical Journal*, *929*(2), 142. doi: 10.3847/1538-4357/ac5d3e

Zhang, L. Q., Lui, A. T., Baumjohann, W., Wang, C., Burch, J. L., & Khotyaintsev, Y. V. (2020). Anisotropic Vorticity Within Bursty Bulk Flow Turbulence. *Journal of Geophysical Research: Space Physics*, *125*(10), 1–9. doi: 10.1029/2020JA028255

Figure 1.

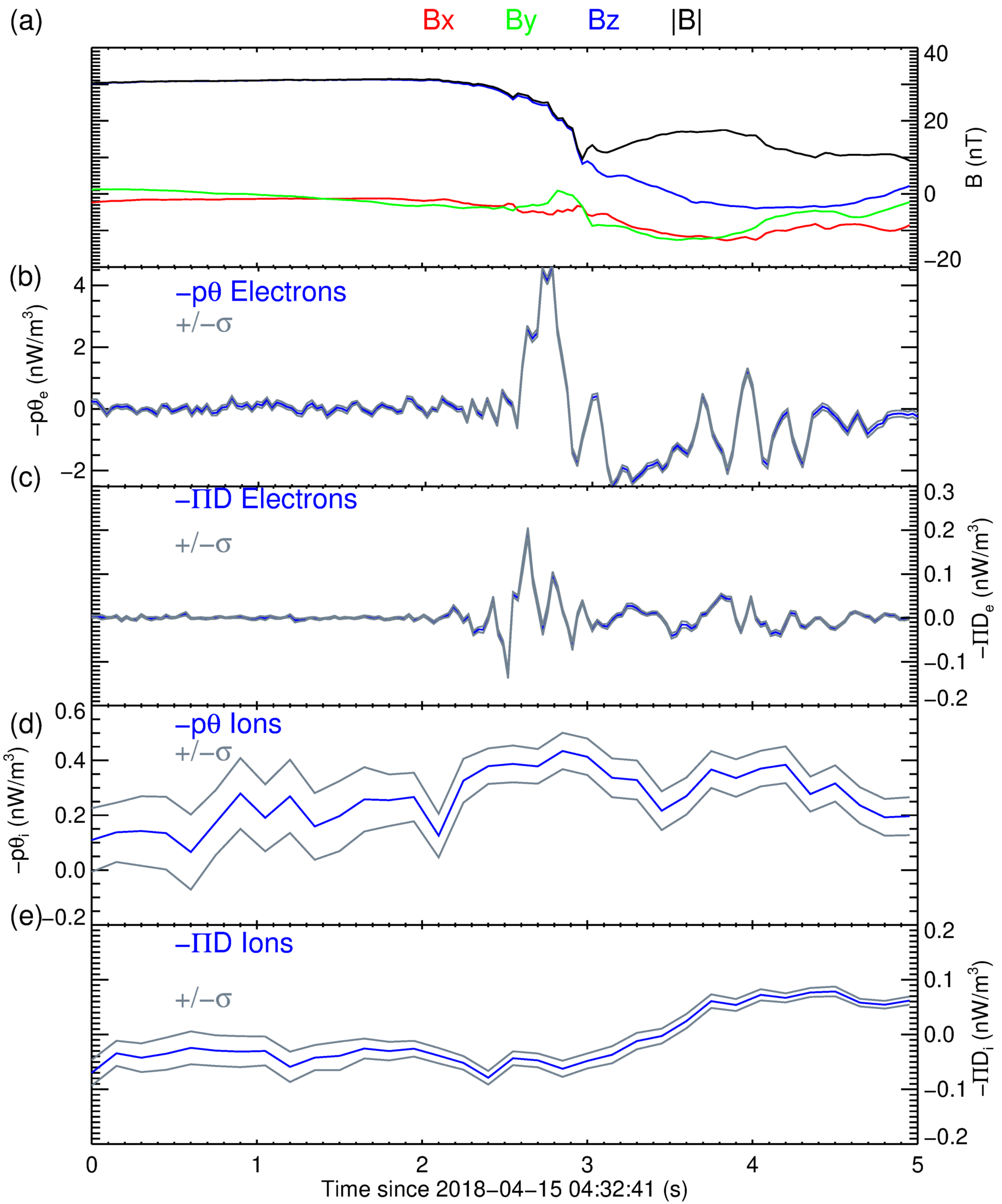

(a)
Bx By Bz |B|
40
20
0
−20
B (nT)
(b)
−pθ Electrons
+/−σ
4
2
0
−2
$-p\theta_e$ (nW/m^3)
(c)
−ΠD Electrons
+/−σ
0.3
0.2
0.1
0.0
−0.1
−0.2
$-\Pi D_e$ (nW/m^3)
(d)
−pθ Ions
+/−σ
0.6
0.4
0.2
0.0
−0.2
$-p\theta_i$ (nW/m^3)
(e)
−ΠD Ions
+/−σ
0.2
0.1
0.0
−0.1
−0.2
$-\Pi D_i$ (nW/m^3)
0
1
2
3
4
5
Time since 2018−04−15 04:32:41 (s)

Figure 2.

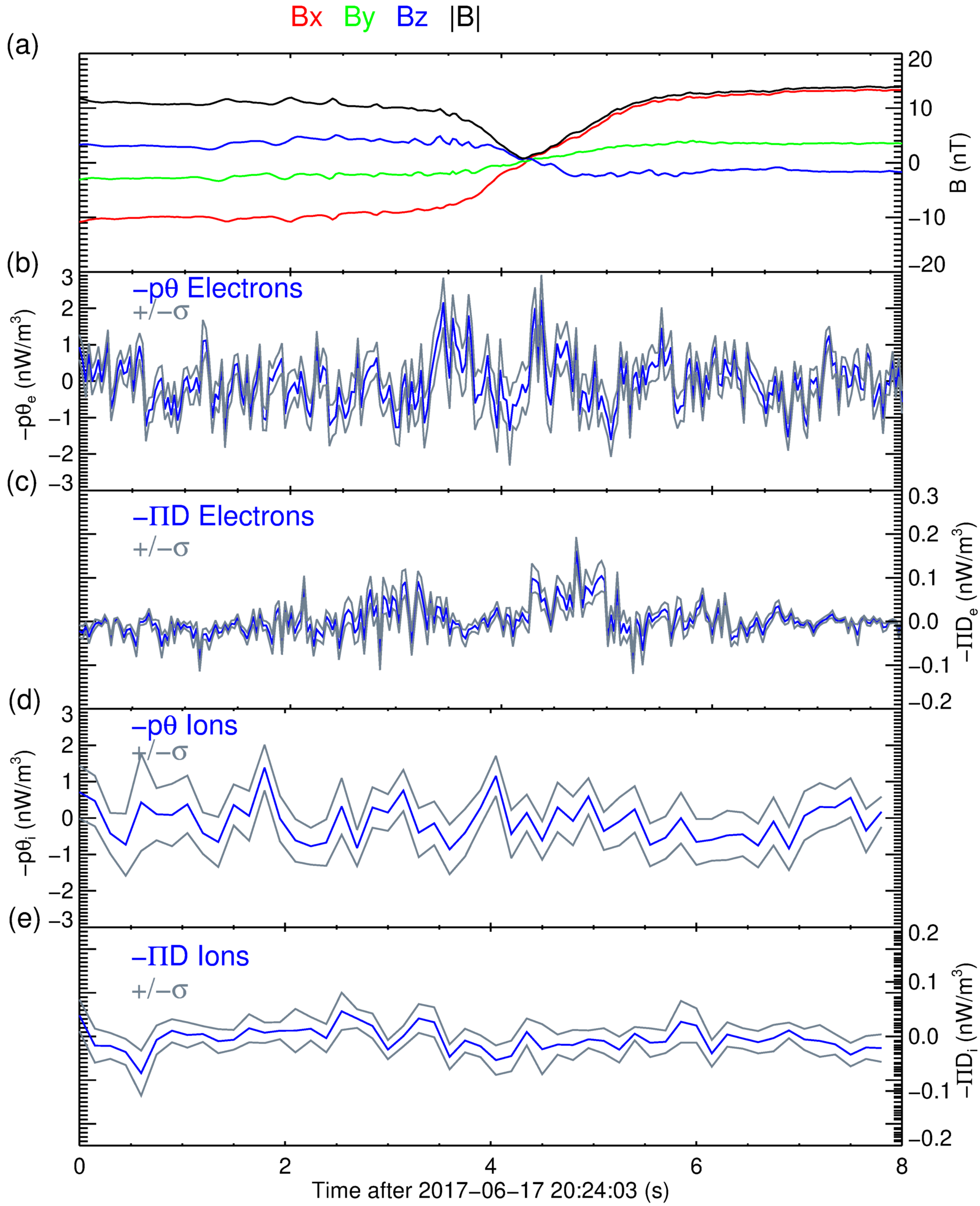

Bx By Bz |B|
(a)
B (nT)
20
10
0
−10
−20
(b)
−pθ Electrons
+/−σ
$-p\theta_e$ (nW/m^3)
(c)
−ΠD Electrons
+/−σ
$-\Pi D_e$ (nW/m^3)
(d)
−pθ Ions
+/−σ
$-p\theta_i$ (nW/m^3)
(e)
−ΠD Ions
+/−σ
$-\Pi D_i$ (nW/m^3)
Time after 2017−06−17 20:24:03 (s)

Figure 3.

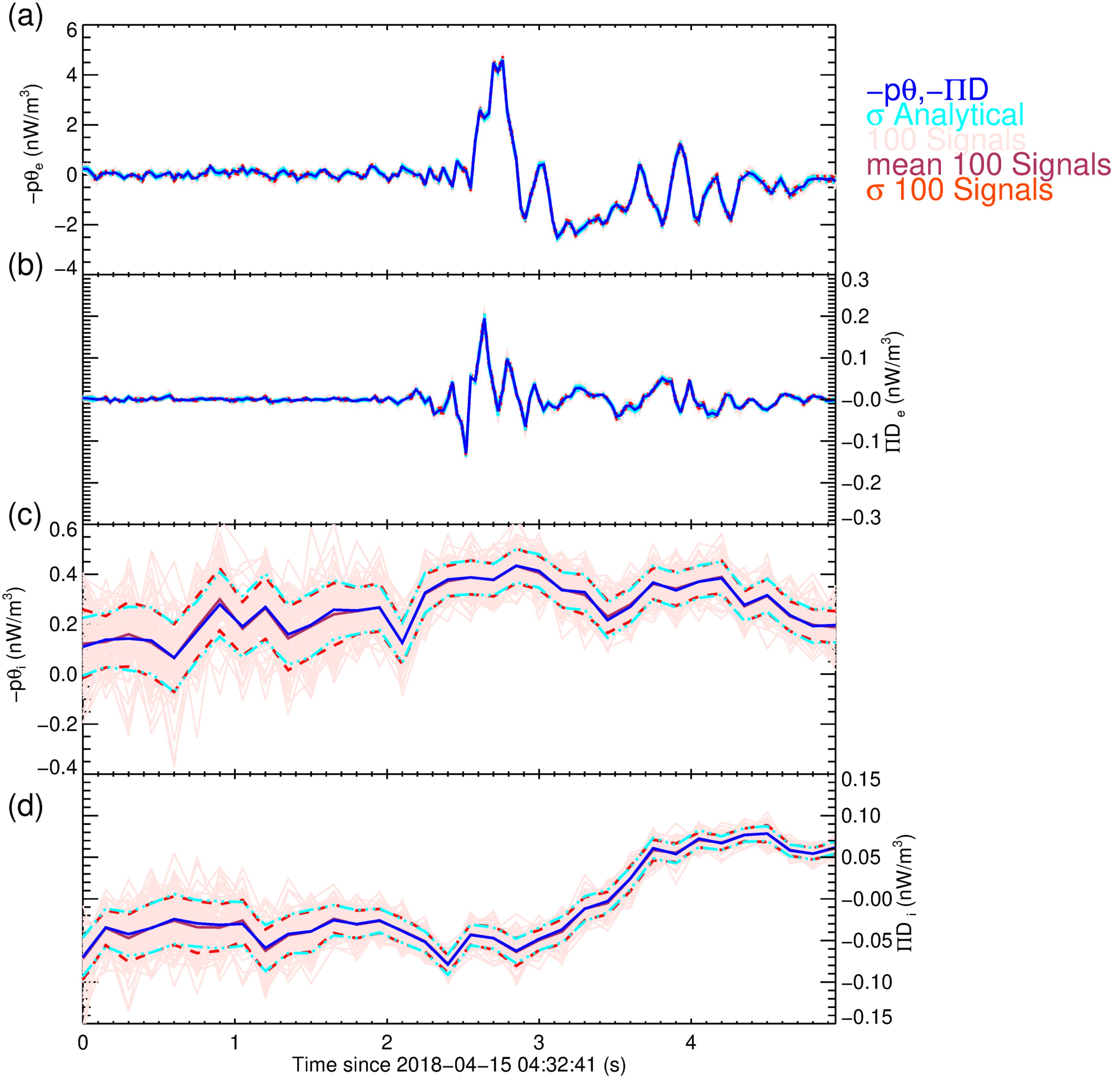

(a)
(b)
(c)
(d)
−pθ,−ΠD
σ Analytical
100 Signals
mean 100 Signals
σ 100 Signals
$-p\theta_e$ (nW/m^3)
ΠD_e (nW/m^3)
$-p\theta_i$ (nW/m^3)
ΠD_i (nW/m^3)
Time since 2018−04−15 04:32:41 (s)

Figure 4.

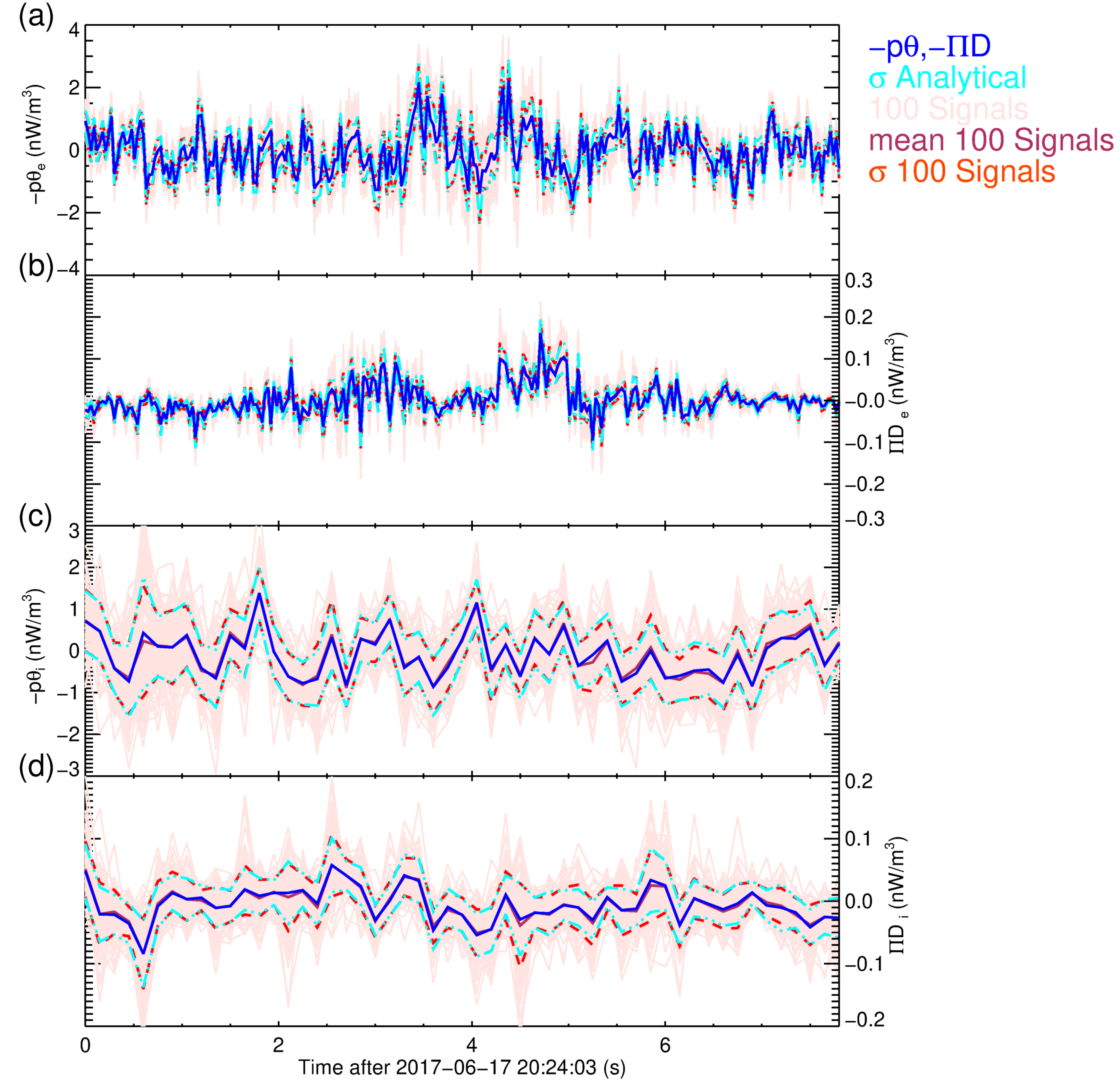
(a)
(b)
(c)
(d)
$-p\theta_e$ (nW/m^3)
ΠD_e (nW/m^3)
$-p\theta_i$ (nW/m^3)
ΠD_i (nW/m^3)
$-p\theta, -\Pi D$
σ Analytical
100 Signals
mean 100 Signals
σ 100 Signals
Time after 2017−06−17 20:24:03 (s)

Figure 5.

(a)
(b)
(c)
El.Density[cm^-3]
Rel.Vi Error
Rel.Ve Error
Ygse [Re]
Xgse [Re]